Geophysical Research Letters

RESEARCH LETTER
10.1029/2020GL089375

Global River Discharge and Floods in the Warmer Climate of the Last Interglacial

Paolo Scussolini[1], Dirk Eilander[1], Edwin H. Sutanudjaja[2], Hiroaki Ikeuchi[3,4], Jannis M. Hoch[2], Philip J. Ward[1], Pepijn Bakker[5], Bette L. Otto-Bliesner[6], Chuncheng Guo[7], Christian Stepanek[8], Qiong Zhang[9], Pascale Braconnot[10], Maria-Vittoria Guarino[11], Sanne Muis[1,12], Dai Yamazaki[3,13], Ted I. E. Veldkamp[1,14], and Jeroen C. J. H. Aerts[1]

[1]Institute for Environmental Studies, Vrije Universiteit Amsterdam, Amsterdam, Netherlands, [2]Department of Physical Geography, Faculty of Geosciences, Utrecht University, Utrecht, Netherlands, [3]Institute of Industrial Sciences, University of Tokyo, Tokyo, Japan, [4]Now at Ministry of Land, Infrastructure, Transport and Tourism, Kyoto, Japan, [5]Earth and Climate Cluster, Vrije Universiteit Amsterdam, Amsterdam, Netherlands, [6]National Center for Atmospheric Research, Boulder, CO, USA, [7]NORCE Norwegian Research Centre, Bjerknes Centre for Climate Research, Bergen, Norway, [8]Alfred Wegener Institute-Helmholtz Centre for Polar and Marine Research, Bremerhaven, Germany, [9]Department of Physical Geography, Stockholm University, Stockholm, Sweden, [10]Laboratoire des Sciences du Climat et de l'Environnement, Université Paris-Saclay, Gif-sur-Yvette, France, [11]British Antarctic Survey, Cambridge, UK, [12]Deltares, Delft, Netherlands, [13]Department of Integrated Climate Change Projection Research, Japan Agency for Marine-Earth Science and Technology, Yokohama, Japan, [14]Now at Urban Technology, Amsterdam University of Applied Sciences, Amsterdam, Netherlands

Key Points:
- We present the first modeling of hydrology and floods for the last interglacial
- Boreal precipitation and runoff are higher than preindustrial, and boreal river discharge and flood volume are (in %) even higher
- Most of the discharge occurs later in the year in large river basins of the Northern Hemisphere

Supporting Information:
- Supporting Information S1

Correspondence to:
P. Scussolini,
paolo.scussolini@vu.nl

Citation:
Scussolini, P., Eilander, D., Sutanudjaja, E. H., Ikeuchi, H., Hoch, J. M., Ward, P. J., et al. (2020). Global River discharge and floods in the warmer climate of the last interglacial. *Geophysical Research Letters*, *47*, e2020GL089375. https://doi.org/10.1029/2020GL089375

Received 19 JUN 2020
Accepted 19 AUG 2020
Accepted article online 25 AUG 2020

Abstract We investigate hydrology during a past climate slightly warmer than the present: the last interglacial (LIG). With daily output of preindustrial and LIG simulations from eight new climate models we force hydrological model PCR-GLOBWB and in turn hydrodynamic model CaMa-Flood. Compared to preindustrial, annual mean LIG runoff, discharge, and 100-yr flood volume are considerably larger in the Northern Hemisphere, by 14%, 25%, and 82%, respectively. Anomalies are negative in the Southern Hemisphere. In some boreal regions, LIG runoff and discharge are lower despite higher precipitation, due to the higher temperatures and evaporation. LIG discharge is much higher for the Niger, Congo, Nile, Ganges, Irrawaddy, and Pearl and lower for the Mississippi, Saint Lawrence, Amazon, Paraná, Orange, Zambesi, Danube, and Ob. Discharge is seasonally postponed in tropical rivers affected by monsoon changes. Results agree with published proxies on the sign of discharge anomaly in 15 of 23 sites where comparison is possible.

Plain Language Summary It is still uncertain how the water cycle will respond to a warmer climate in the coming decades. To increase our understanding of the relationships between climate and hydrology, we study the past climate of the last interglacial, which was slightly warmer than the present. We present the results of a modeling approach, showing that while Northern Hemisphere precipitation was higher during the last interglacial, discharge of rivers was even higher, and floods were even larger. On the contrary, in the Southern Hemisphere precipitation, discharge and floods were lower. We show that, for some regions, precipitation, discharge, and floods do not have the same direction of change. The seasonal timing of discharge also changes for some large basins of the Northern Hemisphere. Finally, for 23 sites, we compare our results to geological evidence. These results form a useful term of comparison to both projections of the future and geological studies of past hydrology.

1. Introduction

With ongoing climate change, the need is pressing to anticipate the response of the hydrological cycle to increasing global temperatures. This can be achieved through modeling frameworks that include emission scenarios and simulation of climate, hydrology, and river hydrodynamics (Arnell & Gosling, 2016; Hirabayashi et al., 2013; van Vliet et al., 2013; Ward et al., 2017). One opportunity to increase our grasp of the Earth's hydroclimate is offered by studying past responses of hydrological systems to different climate states that occurred during the Earth's history, on which geology grants evidence (Harrison et al., 2015; Lunt, Elderfield, et al., 2013). As climate swung between glacials and interglacials of the Quaternary,

global, or at least hemispheric, temperatures sometimes exceeded those of the present day (PAGES, 2016). The most recent of those intervals is the last interglacial (LIG; 129 to 116 kyr ago). The LIG holds special relevance to the future, because of the unique combination of two factors: its proximity in geological time, which means that the conditions of most climate system components are comparable to the present, and its partial temperature analogy with possible futures. Atmospheric surface temperatures were higher than the preindustrial (PI) period and probably slightly higher than the present, with largest anomalies in the Northern Hemisphere and particularly at its high latitudes (CAPE Members, 2006; Turney & Jones, 2010); however, global quantifications are still inadequate (Capron et al., 2017). Global estimates of LIG sea surface temperature anomalies compared to the present range between 0°C and +0.9°C (Hoffman et al., 2017; Turney et al., 2020) and mean ocean temperature anomaly is estimated to be approximately +1°C (Shackleton et al., 2020). The warmth of the LIG was due to the different latitudinal distribution of seasonal insolation and the resulting internal climate feedbacks, principally related to Arctic amplification of warming. The LIG has been abundantly studied in terms of temperature, using climate models (e.g., Lunt, Abe-Ouchi, et al., 2013; Otto-Bliesner et al., 2013, 2020) and with proxies covering some Northern Hemisphere continents and many ocean subbasins (Capron et al., 2017; Hoffman et al., 2017; Turney et al., 2020), and recently also in terms of precipitation (Nikolova et al., 2013; Pedersen et al., 2017). In particular, the higher boreal LIG precipitation likely resulted from high-latitude warming and associated reduction in boreal latitudinal temperature gradients, ultimately linked to differences in insolation (Scussolini et al., 2019). While reconstructions of LIG runoff and river discharge are available for some locations (supporting information Table S1), for example, for the Nile (Wu et al., 2018) and Congo rivers (Gingele et al., 1998), the hydrological implications of the different atmospheric and land climate of the LIG remain unexplored to this day. The application of hydrological modeling to study large-scale changes before the twentieth century is rare. Exceptions are the modeling of Holocene discharge for a set of large river basins (Aerts et al., 2006; Ward et al., 2007).

In this study we (1) model global anomalies between LIG and PI surface runoff, river discharge, and floods; (2) validate those anomalies by comparison with the available proxies; and (3) quantify modeled anomalies of hydrological extremes, in discharge and floods. To these ends, we use results from the latest generation of climate models to force state-of-the-art global hydrological and hydrodynamic models. Our discharge and flood results form the first global picture of hydrological conditions for the LIG.

2. Materials and Methods

To simulate the hydrology and hydrodynamics of the LIG and the PI, we use data from eight global climate models of the Paleoclimate Modelling Intercomparison Project Phase 4: CESM1.2, CESM2, EC-EARTH3.2, HadGEM3-GC3.1, IPSL-CM6-LR, MPI-ESM 1.2.01p1-LR, NorESM1-F, and NUIST-CSM. Depending on the model, the atmosphere's resolution ranges from 1° to 2°, and simulations last between 100 and 300 yr. Simulations are conducted at equilibrium conditions, with forcing reflecting 127 ka for the LIG and CE 1850 for the PI. From the climate models, daily total precipitation and near-surface air temperature are inputted in the global hydrological model PCR-GLOBWB Version 2 (Sutanudjaja et al., 2018). We test the climate model data against climate reanalysis (Text S2 and Figures S1 and S2) and determine that bias correction of climate variables prior to input in the hydrological model is not warranted. Input data are bilinearly interpolated to the 0.5° resolution of the hydrological simulations. The time step is daily. Potential reference evapotranspiration is calculated from air temperature using the Hamon method (Hamon, 1963). Simulations reflect natural conditions as much as possible, and human factors are excluded. Both LIG and PI simulations use present-day maps for land cover, river networks, and sea levels. In hydrological simulations, we let the groundwater storage adjust to the different climatology and then spin up the model for 50 yr. From PCR-GLOBWB we analyze surface runoff. We then interpolate the daily surface runoff from PCR-GLOBWB for input into the global hydrodynamic model CaMa-Flood (Yamazaki et al., 2011), which solves the local inertial equation and runs at 0.25° resolution. From CaMa-Flood's output we analyze routed river discharge, flood (inundated) area, and flood volume (i.e., flood area × flood depth) per grid cell. All variables are averaged across the whole model time series, unless specified. Further, we investigate changes at the river basin scale, for 27 major rivers selected to approximately cover all climatic regions (Figure S10). We report anomalies in seasonal discharge at the river mouth in the form of average annual hydrographs, along the boreal water year (October to September). To correctly compare the two simulations, we account for the seasonal implications of a different Earth's orbit during the LIG by applying the angular definition of

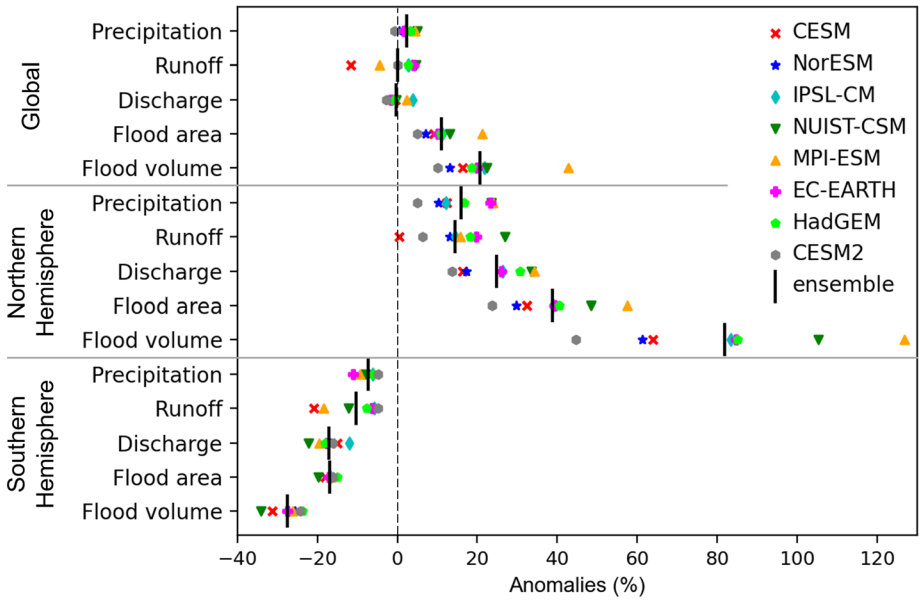

Figure 1. Summary of area-weighted global and hemispheric percentage anomalies between last interglacial and preindustrial simulations, for each model and for the ensemble mean. Precipitation is calculated over land only. Values are averaged across the entire time series, from daily values (precipitation, runoff, and discharge) and from annual maxima (flood area and flood volume).

calendar (Bartlein & Shafer, 2019). See Text S1 for additional details on each model and simulation and Text S2 and Figures S3–S5 for a test of the sensitivity of our results with respect to bias correction of the climate data sets.

3. Results

3.1. Large-Scale Patterns of Runoff and Discharge

Compared to the PI simulation, the global area-weighted average precipitation rate for the LIG displays slightly positive anomaly (i.e., rate is higher in the LIG than in the PI), namely, an ensemble mean of +2.3% (with −0.6% to +5.0% intermodel spread) (Figure 1). This results in negligible runoff anomaly of +0.1% (−11.7% to +4.7%) and negligible anomaly of the routed river discharge of −0.2% (−2.7% to +3.8%). In the Northern Hemisphere anomalies are consistently positive: +16% (+5% to +24%) for precipitation, +14% (+1% to +27%) for runoff, and +25% (+14% to +34%) for discharge. Conversely, in the Southern Hemisphere negative LIG precipitation anomaly of −7.3% (−4.9% to −11.1%) results in negative runoff anomaly of −10% (−21% to −5%) and in more negative discharge anomaly of −17% (−22% to −12%). Intermodel spreads are wider in the Northern Hemisphere.

For the vast majority of regions, anomalies of LIG runoff and precipitation coincide in sign (Figure 2). In departure from this rule, some areas present negative runoff anomaly where LIG precipitation is positive, mostly over eastern and northern Asia, northern continental Canada, northern South America, and Iberian Peninsula. In most of these cases, the LIG runoff coefficient is lower (Figure S7), indicating that a smaller portion of precipitation converts into runoff. This is mainly a result of higher evaporation (Figure S9) due to higher air temperature (Figure S6). Comparing anomalies in discharge (Figures 3 and S11) and precipitation, areas where negative LIG discharge corresponds to positive precipitation are found mostly over northeast Asia (Amur and Lena river basins), northern Canada, and the east coast of North America; positive discharge corresponds to negative precipitation over smaller areas: mainly northeast Brazil, northwestern North America, and Madagascar. Last, comparing runoff and discharge, areas of positive discharge anomaly and negative runoff emerge mostly over northeast Asia, northern South America, Iberian Peninsula, and central Asia, whereas small areas of negative discharge and positive runoff are found over East and central Asia, northern North America, and southern Australia.

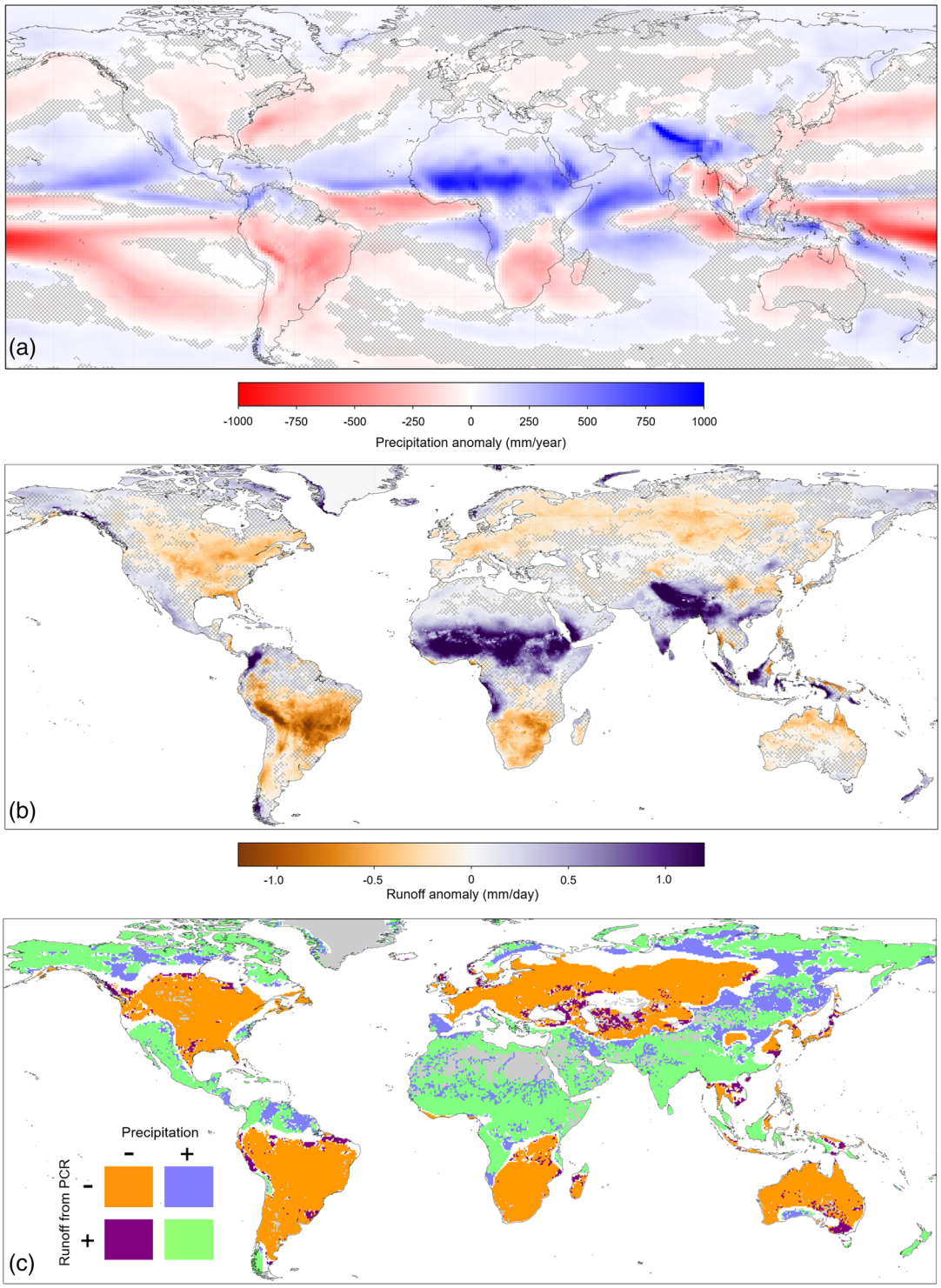

Figure 2. Ensemble anomaly in annual mean precipitation from the climate models (a) and in surface runoff from hydrological model PCR-GLOBWB (b). Areas for which more than two models (out of eight) disagree with the sign of the anomaly in precipitation and runoff are hatched. Also shown (c) are areas where the sign of anomalies in precipitation and runoff coincides or diverges, in a discrete color scale; white indicates that either percentage anomaly is comprised between −2% and +2%; gray indicates no runoff values.

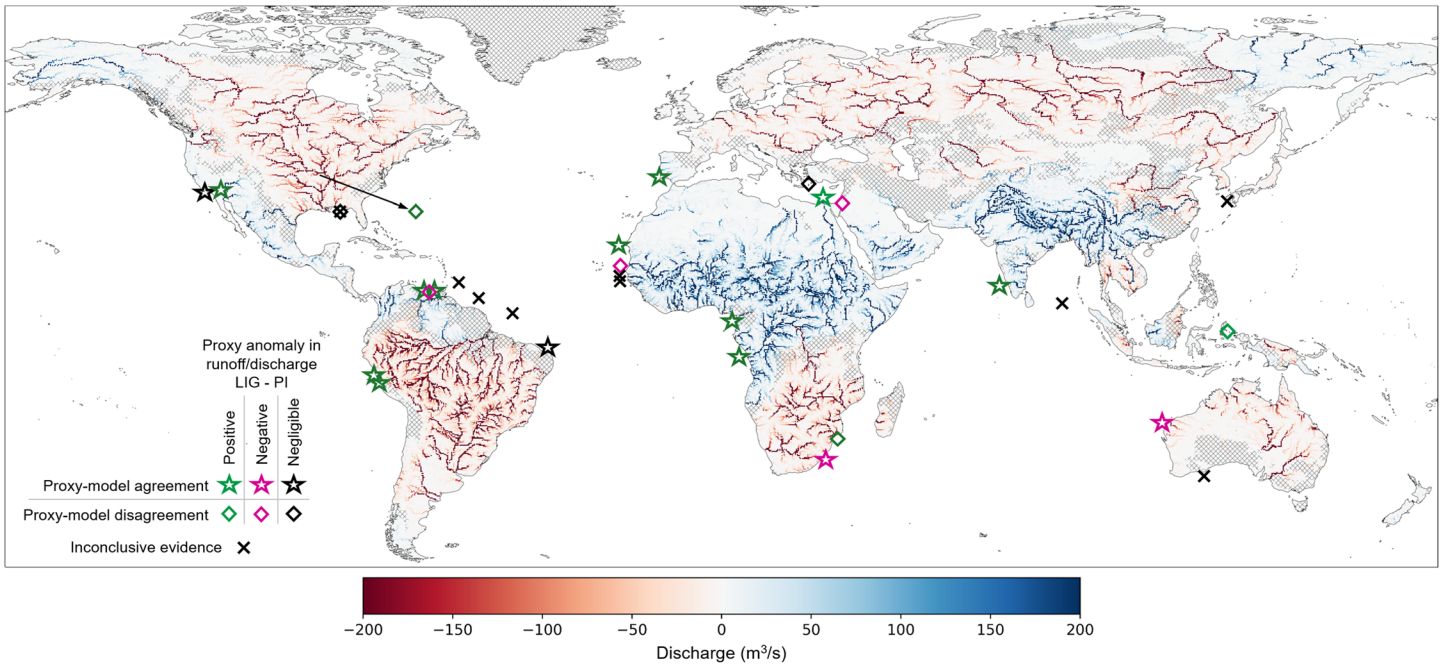

Figure 3. Ensemble anomaly in river discharge from hydrodynamic model CaMa-Flood, along with river discharge from published proxies, in markers. Hatching as per Figure 2. Green (purple) stars and diamonds indicate positive (negative) anomalies from the proxies. Stars (diamonds) indicate agreement (disagreement) with the model ensemble in the sign of anomaly. The arrow indicates the location of the proxy record in the Mississippi basin. Details and references of proxy records are in Table S1. Discharge from hydrological model PCR-GLOBWB is shown in Figure S8 for reference.

3.2. Annual and Seasonal Discharge of Main Rivers

Annual hydrographs show much higher discharge at the river mouth in the LIG than PI for basins in Africa: Nile, Niger, and Jubba-Shebelle (Figure 4). LIG discharge is clearly higher almost year-round for the Congo, Irrawaddy, Lerma-Santiago, and Douro. It is clearly lower for rivers Flinders, Murray-Darling, Zambesi, Orange, Paraná, Amazon, Mississippi, Saint Lawrence, Danube, and Ob and slightly lower for the Yenisei, Rhine, and Mackenzie. A common pattern is that several rivers with higher LIG yearly discharge display somewhat negative anomalies in spring/summer: the Ganges-Brahmaputra-Meghna, Pearl, Lena, and Anadyr. The opposite happens for the Rhine and Mackenzie, where positive summer anomalies emerge amidst annually negative anomalies. Intermodel spread in the percent anomaly of seasonal and annual discharge varies across rivers and tends to be larger in regions with higher LIG precipitation, runoff, and discharge: in the North African monsoon and adjacent region (Nile, Niger, and Jubba-Shebelle), in the Indian monsoon (Ganges-Brahmaputra-Meghna, Irrawaddy), in the South American monsoon (Orinoco), and in northeast Asia (Lena, Anadyr). An exception is the large intermodel spread for the Murray-Darling, where precipitation and runoff anomalies also diverge across models (Figure 2).

For most basins, the seasonal pattern of discharge is similar across LIG and PI simulations, except from some rivers in the tropics, where strong changes in the timing of monsoonal precipitation and in the domains of monsoons (Scussolini et al., 2019) result in a different shape of the hydrograph. Seasonality changes notably for the Congo, where a bimodal LIG hydrograph substitutes a near-unimodal PI one. For several basins, the seasonal contrast in discharge is stronger in the LIG, for example, for the Orinoco, Douro, Rhine, Ganges-Brahmaputra-Meghna, Irrawaddy, Yangtze, and Pearl. Furthermore, in many basins the peak of annual discharge is shifted forward, by days up to weeks: in the Amazon, Orange, Zambesi, Mississippi, Saint Lawrence, Douro, Danube, Rhine, and Yangtze.

To represent changes in the annual timing of discharge, we inspect changes in the timing of the annual center of mass of flow (CMF) (Stewart et al., 2005) (bottom lines in Figure 4). The CMF of the LIG is anticipated by as much as 42 days in the case of the Niger and postponed by as much as 36 days in the Irrawaddy. In many rivers of the Northern Hemisphere the CMF occurs later in the LIG (Mackenzie, Mississippi, Saint

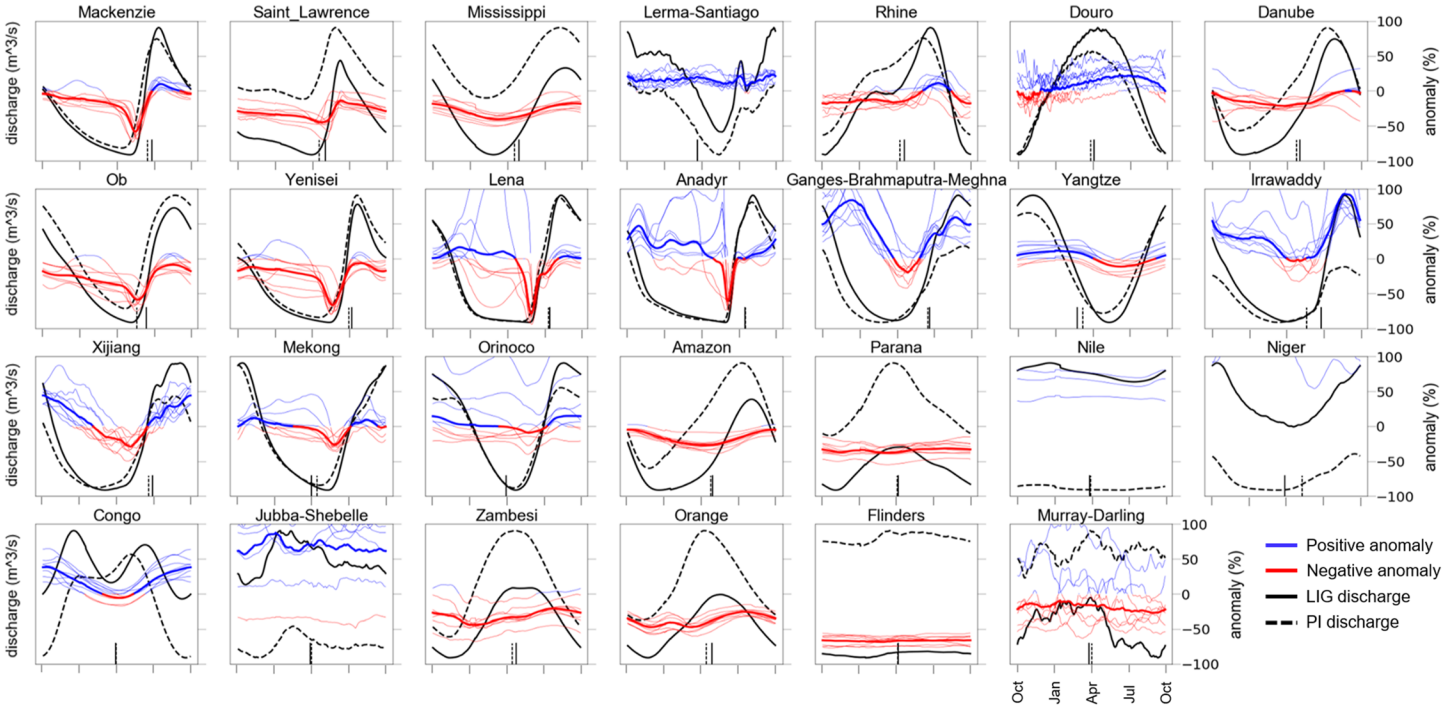

Figure 4. Average annual hydrographs of discharge at points near the mouth of major river basins. *x* axes are days in a "water year" from 1 October to 30 September. Left-hand *y* axis is the ensemble mean value of absolute discharge, for last interglacial (solid black lines) and preindustrial climates (dashed black lines). Axis range is different for each reader and is omitted. Right-hand *y* axis is the percentage anomaly between the two climates, blue for positive (higher discharge during LIG), and red for negative. Individual models are in thin lines, and ensemble means in thick lines. Axis range is −100% to 100%. The vertical lines at the bottom of each panel represent the timing of the annual center of mass of flow, for LIG (solid line) and PI (dashed line). The angular calendar is applied to the LIG data.

Lawrence, Douro, Rhine, Danube, Ob, Irrawaddy, Yenisei, and Pearl), in many cases reflecting enhanced precipitation in summer and early autumn. The Niger and the Yangtze are the only boreal rivers for which LIG CMF occurs substantially earlier. It must be noted that the Niger is also anomalous in that its LIG discharge is +200% larger. In the Southern Hemisphere, the CMF of LIG rivers shifts substantially only in the Orange and Zambesi, where it occurs later, and in the Mekong and Murray-Darling, where it occurs earlier. Although the seasonal pattern changes widely in the Congo, its CMF is virtually the same. In other basins with much higher LIG discharge (Nile and Jubba-Shebelle), the CMF shifts by only 2 days.

3.3. Extreme Discharge and Floods

Global area-weighted average anomalies in annual maxima of flood metrics are more accentuated than anomalies in annual average precipitation, runoff, and discharge (Figure 1). Anomalies in annual maximum of flood volume are larger than flood area. Globally, LIG simulations display +11% (with +5% to +21% intermodel spread) flood area and +21% (+10% to +43%) flood volume. Especially in the Northern Hemisphere, the positive anomalies are very strong, with +39% (+24% to +57%) flood area and +82% flood volume, with very large intermodel spread for the latter: +45% to +127%. For the Southern Hemisphere, anomalies are −17% (−20% to −15%) for flood area and −27% (−34% to −24%) for flood volume. The much larger anomalies of floods metrics cannot be attributed to changes in extreme precipitation (not shown), as these are even smaller than changes in mean precipitation. Geographic patterns of anomalies in flood area and flood volume at the 100-yr return period (Figure S13) diverge in many regions from anomalies in runoff (Figure 2) and discharge (Figure 3), mainly over northern Asia, North America, and India. Also, they are more spatially heterogeneous, pointing to the relevance of subbasin processes to modeled floods. To assess the link between precipitation intensity and hydrological extremes, we calculate annual maximum precipitation in consecutive intervals of 5, 15, and 30 days (Figure S14). In the Northern Hemisphere, geographical coincidence in the sign of anomaly is higher between flood area (or volume) and 5-day maximum precipitation than between flood area (or volume) and average precipitation (Figure S13). This indicates that, in the

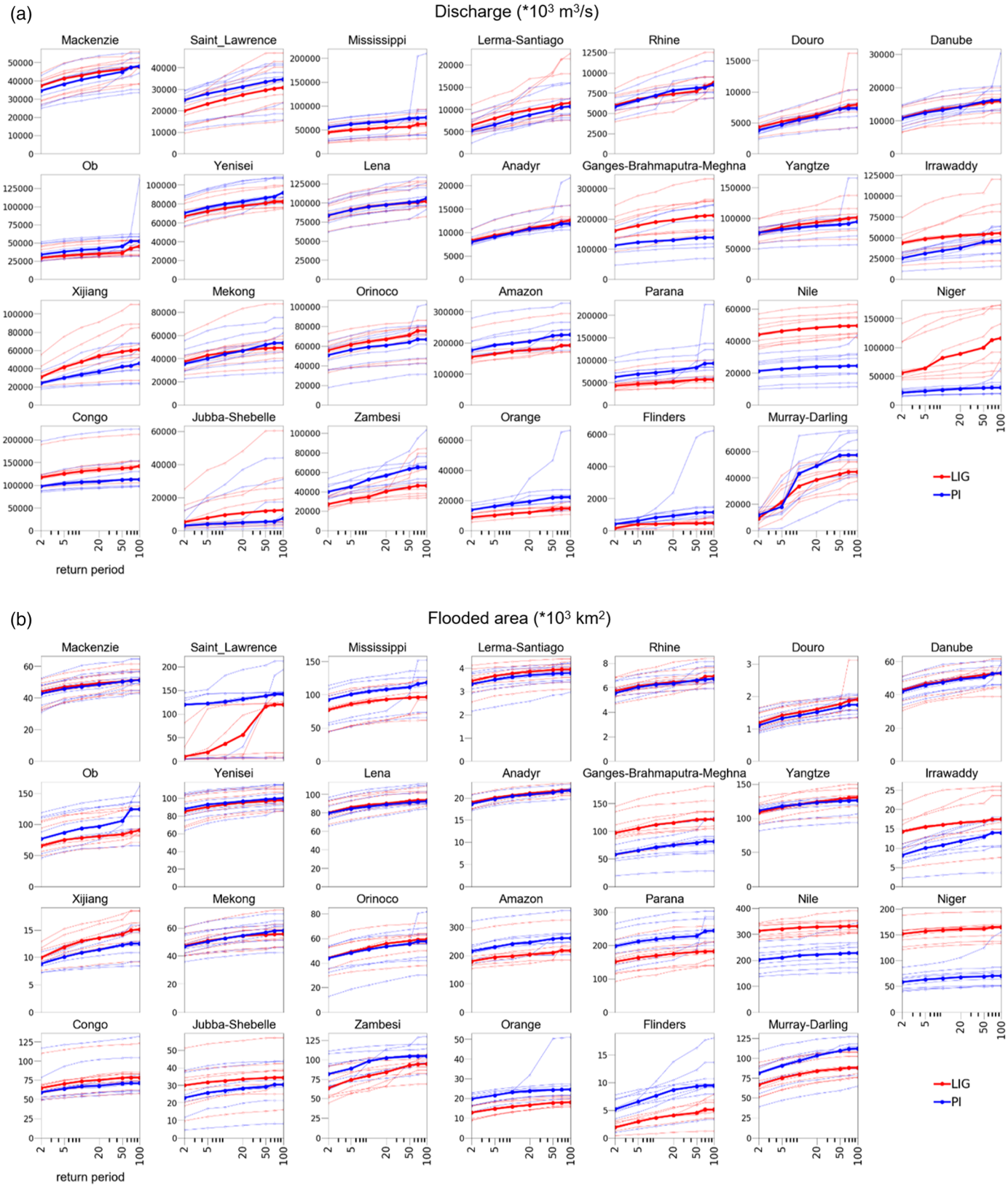

Figure 5. Extremes of discharge (a) and of flood area (b) for main river basins (shown in Figure S5), for a set of return periods from 2 to 100 yr. Red and blue lines represent last interglacial and preindustrial climates, respectively. Individual models are in thin lines, and ensemble means in thick lines. Discharge is calculated for each basin in proximity of the river mouth; flood area is summed for the whole basin.

model, extremes in boreal flooding are driven by intense precipitation over multiple days rather than by average precipitation.

For discharge and flood area in the same river basins analyzed above, the ensemble-averaged extreme values increase from return periods of 2 to 100 yr in a similar fashion (Figure 5; flood volume is omitted because the shape of its curves is comparable to flood area). For most basins, patterns of extremes of intense precipitation are very similar for 5-, 15-, and 30-day intervals and mostly also resemble patterns of extreme discharge and flood area (Figure S.15). Notable deviations from this similarity emerge: (1) in the Mississippi, where LIG discharge and flood are lower than PI, whereas extremes of intense precipitation are virtually the same across simulations; and (2) in the Saint Lawrence and Flinders, where LIG discharge extremes are slightly lower, whereas LIG flood area extremes are much lower.

3.4. Comparison to Proxies of Discharge/Runoff

We revise proxy studies that report patterns of LIG runoff and discharge, to compare to the modeling results. We select mostly records of marine sediments under the influence of either discharge downstream from main river mouths or broadly of runoff from the adjacent land. Often, the interpretation of such records is dubious, because of the presence of multiple mechanisms that may concur to explain the proxy signal, such as strong sea level variations of the glacial-interglacial cycles (e.g., Kujau et al., 2010) and potential shifts in the location of river mouths that are poorly constrained topographically. We find published proxies for 32 sites, of which 23 are suitable for comparison with models (Table S1). The modeled discharge agrees with the proxies on the sign of LIG anomaly at 15 sites: the west coast of North America; the north and west coasts of South America; at several sites on the northern, eastern, and southern coasts of Africa; at the southeast of India; and at western Australia (Figure 3). Disagreement occurs over the Mississippi basin and downstream its river mouth, at the northern coast of South America (where model resolution is likely inadequate to capture small-scale gradients), the western coast of Northern Africa, the eastern Mediterranean region, over the Limpopo basin, and at a site in Indonesia.

4. Discussion and Conclusions

Because reconstructing climatic and hydrological signals from proxies is hard, it is tempting to extend the interpretation of proxies of, for example, precipitation, to also represent hydrological variables as runoff, discharge, and flood, or conversely. Although our model results indicate that for most areas the sign of anomaly in those variables coincides, the discrepancies that emerge for nonnegligible land portions (Figures 2, S11, and S13) provide a cautionary message for the interpretation of proxy records. On the other hand, areas where modeled variables diverge and areas of stronger anomaly could inform site selection for proxy reconstructions that help shed light into mechanisms of LIG hydroclimate.

In the only modeling studies that offer points of paleoclimatic comparison for our results, Aerts et al. (2006) and Ward et al. (2007) simulated discharge for major rivers during the mid-Holocene, when insolation and warming anomalies were geographically comparable, though smaller in magnitude, to those of the LIG. Their annually integrated anomalies agree in sign with our LIG ones for the Ganges, Congo, Lena, Murray-Darling, Amazon, Zambesi, and Nile. They slightly disagree for the Danube, Rhine, and Mekong and completely disagree for the Mississippi. Attributing discrepancies with those results is unattainable because the effect of different climate forcing and very different modeling framework cannot be separated. By virtue of the possible similarities in the geographic pattern of temperature anomalies, another term of comparison for LIG discharge are the ensemble mean results of simulations for the end of this century (2070–2100) under high-emission scenarios, although key differences in forcing between these climates (Bony et al., 2013) limit the merit of this comparison. Our LIG positive discharge anomalies agree with future projections from CMIP3 models (van Vliet et al., 2013) over northeast Asia, Alaska, central Africa, and the Arabian Peninsula. LIG negative discharge anomalies agree over southern Africa and parts of North America and of Europe. Glaring disagreement emerges over Northern Africa and the Mediterranean, tropical South America, Southeast Asia, and particularly the Himalaya region. Compared to CMIP5-based projections, anomalies in LIG discharge hydrographs are similar for Rhine, Ganges, and Yangtze and different for Amazon, Niger, Nile, Mississippi, Mackenzie, and Lena (Krysanova et al., 2017). LIG floods are lower over many parts of Europe, in agreement with CMIP3-based future projections (Arnell & Gosling, 2016) but in disagreement with projections based on downscaled CMIP5 results (Alfieri et al., 2015).

Precipitation is an uncertain product of global climate models (e.g., Huang et al., 2020; see also Text S1). Nevertheless, precipitation from an almost identical ensemble of climate models has been validated by comparison to proxies (Scussolini et al., 2019). That study reports that climate models seem to reasonably reproduce the main features of LIG precipitation, especially in the Northern Hemisphere. Besides, comparison of proxies with a similar ensemble of models shows broad agreement in LIG Arctic amplification of warmer temperatures (Otto-Bliesner et al., 2020). Our proxy-model comparison on discharge and runoff supplies additional confidence in the models' capabilities of reproducing past climate change, suggesting that even for a cascade of climate-hydrological-hydrodynamic models there is more agreement than disagreement with proxies. It must be noted that there are inherent limits of this model-proxy comparison. Beyond those raised by Scussolini et al. (2019), an additional limit derives from the fact that LIG simulations are carried out with current maps of river network, land cover, permafrost, and sea levels. Although these were likely different in the LIG (e.g., the top of the permafrost may have been deeper in warmer boreal climate), improvements in this direction are postponed until global data sets for this period will emerge. Further, although we found more proxies than were found for Holocene discharge (Aerts et al., 2006), these are fewer than for LIG precipitation (Scussolini et al., 2019), and the number of suitable comparisons is too small to draw conclusions about the geographic pattern of model-proxy agreement. Nevertheless, with growing interest and with accelerated development in the fields of paleohydrology and paleo floods (Baker, 2013; Wilhelm et al., 2017, 2018), it is realistic that the coverage and resolution of proxies for runoff, discharge, and flooding will increase, enabling more extensive comparison with the models presented here. Additionally, the above mentioned forms of validation with proxies enable selecting models that best reproduce observations for the LIG and that can therefore be assumed to better capture the internal feedbacks of the climate system in a warmer climate. With ad hoc methodologies, this could in turn enable differential weighting of models in the context of ensemble studies (Eyring et al., 2019).

Lastly, our hydrological results inform the study of the LIG history of ecosystems and humans at the continental scale. For example, humid LIG conditions have been inferred for sectors of North Africa that were crucial to prehistoric human migrations (Larrasoana et al., 2013). The timing of human dispersal from Africa is not well constrained, with current hypotheses based on genomics and archeology suggesting migrations in the time window 130–50 ka, via the Bab el Mandeb strait or the Sinai Peninsula (López et al., 2015), and pioneer hydrodynamic studies indicating possible LIG migration to the Mediterranean along a western route (Coulthard et al., 2013). For 127 ka, increased precipitation emerges from proxies and models over the Sahel, Sahara, Arabian Peninsula, Levant, and Middle East, with further-reaching and longer monsoon seasons (Scussolini et al., 2019). We here simulate higher LIG annual runoff and discharge over North Africa and the southwestern Arabian Peninsula. All this points to the existence of a river network and to greening of key regions that may have sustained the path of human tribes migrating across and out of the continent.

Data Availability Statement

The results of the hydrological and hydrodynamic models that form the basis for the analyses here presented are available as netCDF files at public repository (https://doi.org/10.5281/zenodo.3677737).

Acknowledgments

P. S. acknowledges funding from the NWO (Nederlandse Organisatie voor Wetenschappelijk Onderzoek) under Grant ALWOP.164, and from SCOR under Project COASTRISK. P. W. acknowledges funding from NWO VIDI grant 016.161.324. Hydrological and hydrodynamic simulations were carried out on the Dutch national e-infrastructure (supercomputer Cartesius) with the support of SURF Cooperative. B. L. O.-B. acknowledges the CESM project, which is supported primarily by the National Science Foundation (NSF). This material is based upon work supported by the National Center for Atmospheric Research (NCAR), which is a major facility sponsored by the National Science Fundation under Cooperative Agreement 1852977. Computing and data storage resources, including the Cheyenne supercomputer (doi:http://10.5065/D6RX99HX), were provided by the Computational and Information Systems Laboratory (CISL) at NCAR. Q. Z. acknowledges funding support from Swedish Research Council VR (2013-06476 and 2017-04232). We thank Jian Cao for providing data of climate model NUIST-CSM.

References

Aerts, J. C. J. H., Renssen, H., Ward, P. J., de Moel, H., Odada, E., Bouwer, L. M., & Goosse, H. (2006). Sensitivity of global river discharges under Holocene and future climate conditions. *Geophysical Research Letters*, *33*, L19401. https://doi.org/10.1029/2006GL027493

Alfieri, L., Burek, P., Feyen, L., & Forzieri, G. (2015). Global warming increases the frequency of river floods in Europe. *Hydrology and Earth System Sciences*, *19*(5), 2247–2260. https://doi.org/10.5194/hess-19-2247-2015

Arnell, N. W., & Gosling, S. N. (2016). The impacts of climate change on river flood risk at the global scale. *Climatic Change*, *134*(3), 387–401. https://doi.org/10.1007/s10584-014-1084-5

Baker, V. R. (2013). 9.26 Global Late Quaternary fluvial paleohydrology: With special emphasis on paleofloods and megafloods. In J. F. Shroder (Ed.), *Treatise on geomorphology* (pp. 511–527). San Diego: Academic Press.

Bartlein, P. J., & Shafer, S. L. (2019). Paleo calendar-effect adjustments in time-slice and transient climate-model simulations (PaleoCalAdjust v1.0): Impact and strategies for data analysis. *Geoscientific Model Development*, *12*, 3889–3913.

Bony, S., Bellon, G., Klocke, D., Sherwood, S., Fermepin, S., & Denvil, S. (2013). Robust direct effect of carbon dioxide on tropical circulation and regional precipitation. *Nature Geoscience*, *6*(6), 447–451. https://doi.org/10.1038/ngeo1799

CAPE_Members (2006). Last interglacial Arctic warmth confirms polar amplification of climate change. *Quaternary Science Reviews*, *25*, 1383–1400.

Capron, E., Govin, A., Feng, R., Otto-Bliesner, B. L., & Wolff, E. W. (2017). Critical evaluation of climate syntheses to benchmark CMIP6/PMIP4 127 ka last interglacial simulations in the high-latitude regions. *Quaternary Science Reviews*, *168*, 137–150. https://doi.org/10.1016/j.quascirev.2017.04.019

Coulthard, T. J., Ramirez, J. A., Barton, N., Rogerson, M., & Brucher, T. (2013). Were rivers flowing across the Sahara during the last interglacial? Implications for human migration through Africa. *PLoS ONE*, *8*, e74834.
Eyring, V., Cox, P. M., Flato, G. M., Gleckler, P. J., Abramowitz, G., Caldwell, P., et al. (2019). Taking climate model evaluation to the next level. *Nature Climate Change*, *9*, 102–110.
Gingele, F. X., Müller, P. M., & Schneider, R. R. (1998). Orbital forcing of freshwater input in the Zaire Fan area—Clay mineral evidence from the last 200 kyr. *Palaeogeography, Palaeoclimatology, Palaeoecology*, *138*(1–4), 17–26. https://doi.org/10.1016/S0031-0182(97)00121-1
Hamon, W. R. (1963). Computation of direct runoff amounts from storm rainfall. *International Association of Scientific Hydrology. Publication*, *63*, 52–62.
Harrison, S. P., Bartlein, P. J., Izumi, K., Li, G., Annan, J., Hargreaves, J., et al. (2015). Evaluation of CMIP5 palaeo-simulations to improve climate projections. *Nature Climate Change*, *5*(8), 735–743. https://doi.org/10.1038/nclimate2649
Hirabayashi, Y., Mahendran, R., Koirala, S., Konoshima, L., Yamazaki, D., Watanabe, S., et al. (2013). Global flood risk under climate change. *Nature Climate Change*, *3*(9), 816–821. https://doi.org/10.1038/nclimate1911
Hoffman, J. S., Clark, P. U., Parnell, A. C., & He, F. (2017). Regional and global sea-surface temperatures during the last interglaciation. *Science*, *355*(6322), 276–279. https://doi.org/10.1126/science.aai8464
Huang, F., Xu, Z., & Guo, W. (2020). The linkage between CMIP5 climate models' abilities to simulate precipitation and vector winds. *Climate Dynamics*, *54*, 4953–4970. https://doi.org/10.1007/s00382-020-05259-6
Krysanova, V., Vetter, T., Eisner, S., Huang, S., Pechlivanidis, I., Strauch, M., et al. (2017). Intercomparison of regional-scale hydrological models and climate change impacts projected for 12 large river basins worldwide—A synthesis. *Environmental Research Letters*, *12*(10), 105002. https://doi.org/10.1088/1748-9326/aa8359
Kujau, A., Nürnberg, D., Zielhofer, C., Bahr, A., & Röhl, U. (2010). Mississippi River discharge over the last ~560,000 years—Indications from X-ray fluorescence core-scanning. *Palaeogeography, Palaeoclimatology, Palaeoecology*, *298*(3–4), 311–318. https://doi.org/10.1016/j.palaeo.2010.10.005
Larrasoana, J. C., Roberts, A. P., & Rohling, E. J. (2013). Dynamics of green Sahara periods and their role in hominin evolution. *PLoS ONE*, *8*(10), e76514. https://doi.org/10.1371/journal.pone.0076514
López, S., Van Dorp, L., & Hellenthal, G. (2015). Human dispersal out of Africa: A lasting debate. *Evolutionary Bioinformatics*, 11s2, EBO. S33489.
Lunt, D. J., Abe-Ouchi, A., Bakker, P., Berger, A., Braconnot, P., Charbit, S., et al. (2013). A multi-model assessment of last interglacial temperatures. *Climate of the Past*, *9*, 699–717.
Lunt, D. J., Elderfield, H., Pancost, R., Ridgwell, A., Foster, G. L., Haywood, A., et al. (2013). Warm climates of the past—A lesson for the future? *Philosophical Transactions of the Royal Society A: Mathematical, Physical and Engineering Sciences*, *371*(2001), 20130146. https://doi.org/10.1098/rsta.2013.0146
Nikolova, I., Yin, Q., Berger, A., Singh, U. K., & Karami, M. P. (2013). The last interglacial (Eemian) climate simulated by LOVECLIM and CCSM3. *Climate of the Past*, *9*(4), 1789–1806. https://doi.org/10.5194/cp-9-1789-2013
Otto-Bliesner, B. L., Brady, E. C., Zhao, A., Brierley, C., Axford, Y., Capron, E., et al. (2020). Large-scale features of last interglacial climate: Results from evaluating the lig127k simulations for CMIP6-PMIP4. *Climate of the Past Discussions*, 1–41.
Otto-Bliesner, B. L., Rosenbloom, N., Stone, E. J., McKay, N. P., Lunt, D. J., Brady, E. C., & Overpeck, J. T. (2013). How warm was the last interglacial? New model–data comparisons. *Philosophical Transactions of the Royal Society A: Mathematical, Physical and Engineering Sciences*, *371*.
PAGES, P. I. W. G. O. (2016). Interglacials of the last 800,000 years. *Reviews of Geophysics*, *54*, 162–219. https://doi.org/10.1002/2015RG000482
Pedersen, R. A., Langen, P. L., & Vinther, B. M. (2017). The last interglacial climate: Comparing direct and indirect impacts of insolation changes. *Climate Dynamics*, *48*(9–10), 3391–3407. https://doi.org/10.1007/s00382-016-3274-5
Scussolini, P., Bakker, P., Guo, C., Stepanek, C., Zhang, Q., Braconnot, P., et al. (2019). Agreement between reconstructed and modeled boreal precipitation of the last interglacial. *Science Advances*, *5*, eaax7047.
Shackleton, S., Baggenstos, D., Menking, J. A., Dyonisius, M. N., Bereiter, B., Bauska, T. K., et al. (2020). Global ocean heat content in the last interglacial. *Nature Geoscience*, *13*(1), 77–81. https://doi.org/10.1038/s41561-019-0498-0
Stewart, I. T., Cayan, D. R., & Dettinger, M. D. (2005). Changes toward earlier streamflow timing across western North America. *Journal of Climate*, *18*(8), 1136–1155. https://doi.org/10.1175/JCLI3321.1
Sutanudjaja, E. H., van Beek, R., Wanders, N., Wada, Y., Bosmans, J. H. C., Drost, N., et al. (2018). PCR-GLOBWB 2: A 5 arcmin global hydrological and water resources model. *Geoscientific Model Development*, *11*(6), 2429–2453. https://doi.org/10.5194/gmd-11-2429-2018
Turney, C. S. M., Jones, R., McKay, N. P., van Sebille, E., Thomas, Z. A., Hillenbrand, C. D., & Fogwill, C. J. (2020). A global mean sea-surface temperature dataset for the last interglacial (129–116 kyr) and contribution of thermal expansion to sea-level change. *Earth System Science Data Discussions*, *2020*, 1–21.
Turney, C. S. M., & Jones, R. T. (2010). Does the Agulhas current amplify global temperatures during super-interglacials? *Journal of Quaternary Science*, *25*(6), 839–843. https://doi.org/10.1002/jqs.1423
van Vliet, M. T. H., Franssen, W. H. P., Yearsley, J. R., Ludwig, F., Haddeland, I., Lettenmaier, D. P., & Kabat, P. (2013). Global river discharge and water temperature under climate change. *Global Environmental Change*, *23*(2), 450–464. https://doi.org/10.1016/j.gloenvcha.2012.11.002
Ward, P. J., Aerts, J. C. J. H., de Moel, H., & Renssen, H. (2007). Verification of a coupled climate-hydrological model against Holocene palaeohydrological records. *Global and Planetary Change*, *57*(3–4), 283–300. https://doi.org/10.1016/j.gloplacha.2006.12.002
Ward, P. J., Jongman, B., Aerts, J. C. J. H., Bates, P. D., Botzen, W. J. W., Diaz Loaiza, A., et al. (2017). A global framework for future costs and benefits of river-flood protection in urban areas. *Nature Climate Change*, *7*(9), 642–646. https://doi.org/10.1038/nclimate3350
Wilhelm, B., Ballesteros Canovas, J. A., Ahlborn, M., Baker, V., Benito, G., Francus, P., et al. (2017). PAGES Floods Working Group—White paper, 2017. Retrieved from http://pastglobalchanges.org/download/docs/working_groups/floods/fwg-white-paper-Nov-17.pdf
Wilhelm, B., Ballesteros Canovas, J. A., Corella Aznar, J. P., Kämpf, L., Swierczynski, T., Stoffel, M., et al. (2018). Recent advances in paleoflood hydrology: From new archives to data compilation and analysis. *Water Security*, *3*, 1–8. https://doi.org/10.1016/j.wasec.2018.07.001
Wu, J., Filippidi, A., Davies, G. R., & de Lange, G. J. (2018). Riverine supply to the eastern Mediterranean during last interglacial sapropel S5 formation: A basin-wide perspective. *Chemical Geology*, *485*, 74–89. https://doi.org/10.1016/j.chemgeo.2018.03.037
Yamazaki, D., Kanae, S., Kim, H., & Oki, T. (2011). A physically based description of floodplain inundation dynamics in a global river routing model. *Water Resources Research*, *47*, W04501. https://doi.org/10.1029/2010WR009726

References From The Supporting Information

Alfieri, L., Bisselink, B., Dottori, F., Naumann, G., de Roo, A., Salamon, P., et al. (2017). Global projections of river flood risk in a warmer world. *Earth's Future*, *5*, 171–182. https://doi.org/10.1002/2016EF000485

Bai, P., Liu, X., Yang, T., Li, F., Liang, K., Hu, S., & Liu, C. (2016). Assessment of the influences of different potential evapotranspiration inputs on the performance of monthly hydrological models under different climatic conditions. *Journal of Hydrometeorology*, *17*(8), 2259–2274. https://doi.org/10.1175/JHM-D-15-0202.1

Bates, P. D., Horritt, M. S., & Fewtrell, T. J. (2010). A simple inertial formulation of the shallow water equations for efficient two-dimensional flood inundation modelling. *Journal of Hydrology*, *387*(1–2), 33–45. https://doi.org/10.1016/j.jhydrol.2010.03.027

Bloemsma, M. R., Zabel, M., Stuut, J. B. W., Tjallingii, R., Collins, J. A., & Weltje, G. J. (2012). Modelling the joint variability of grain size and chemical composition in sediments. *Sedimentary Geology*, *280*, 135–148. https://doi.org/10.1016/j.sedgeo.2012.04.009

Brewer, S., Guiot, J., Sánchez-Goñi, M. F., & Klotz, S. (2008). The climate in Europe during the Eemian: A multi-method approach using pollen data. *Quaternary Science Reviews*, *27*(25–26), 2303–2315. https://doi.org/10.1016/j.quascirev.2008.08.029

Brodie, I., & Kemp, A. E. S. (1994). Variation in biogenic and detrital fluxes and formation of laminae in late Quaternary sediments from the Peruvian coastal upwelling zone. *Marine Geology*, *116*(3–4), 385–398. https://doi.org/10.1016/0025-3227(94)90053-1

Caley, T., Extier, T., Collins, J. A., Schefuß, E., Dupont, L., Malaizé, B., et al. (2018). A two-million-year-long hydroclimatic context for hominin evolution in southeastern Africa. *Nature*. https://doi.org/10.1038/s41586-018-0309-6

Clemens, S. C., Holbourn, A., Kubota, Y., Lee, K. E., Liu, Z., Chen, G., et al. (2018). Precession-band variance missing from East Asian monsoon runoff. *Nature Communications*, *9*(1), 3364. https://doi.org/10.1038/s41467-018-05814-0

Collins, M., Knutti, R., Arblaster, J., Dufresne, J. L., Fichefet, T., Friedlingstein, P., et al. (2013). Long-term climate change: Projections, commitments and irreversibility. In T. F. Stocker, et al. (Eds.), *Climate change 2013: The physical science basis. Contribution of Working Group I to the Fifth Assessment Report of the Intergovernmental Panel on Climate Change*. Cambridge, UK: Cambridge University press.

Compo, G. P., Whitaker, J. S., Sardeshmukh, P. D., Matsui, N., Allan, R. J., Yin, X., et al. (2011). The Twentieth Century Reanalysis Project. *Quarterly Journal of the Royal Meteorological Society*, *137*, 1–28.

Contreras, S., Lange, C. B., Pantoja, S., Lavik, G., Rincón-Martínez, D., & Kuypers, M. M. M. (2010). A rainy northern Atacama Desert during the last interglacial. *Geophysical Research Letters*, *37*, L23612. https://doi.org/10.1029/2010GL045728

Dang, H., Jian, Z., Kissel, C., & Bassinot, F. (2015). Precessional changes in the western equatorial Pacific hydroclimate: A 240 kyr marine record from the Halmahera Sea, East Indonesia. *Geochemistry, Geophysics, Geosystems*, *16*, 148–164. https://doi.org/10.1002/2014GC005550

Eyring, V., Bony, S., Meehl, G. A., Senior, C. A., Stevens, B., Stouffer, R. J., & Taylor, K. E. (2016). Overview of the Coupled Model Intercomparison Project Phase 6 (CMIP6) experimental design and organization. *Geoscientific Model Development*, *9*(5), 1937–1958. https://doi.org/10.5194/gmd-9-1937-2016

FAO (2007). Digital soil map of the world, Version 3.6, Food and Agriculture Organization of the United Nations (FAO), Rome, Italy.

Federer, C. A., Vörösmarty, C., & Fekete, B. (1996). Intercomparison of methods for calculating potential evaporation in regional and global water balance models. *Water Resources Research*, *32*(7), 2315–2321. https://doi.org/10.1029/96WR00801

Fischer, E. M., & Knutti, R. (2016). Observed heavy precipitation increase confirms theory and early models. *Nature Climate Change*, *6*(11), 986–991. https://doi.org/10.1038/nclimate3110

Fischer, E. M., Sedláček, J., Hawkins, E., & Knutti, R. (2014). Models agree on forced response pattern of precipitation and temperature extremes. *Geophysical Research Letters*, *41*, 8554–8562. https://doi.org/10.1002/2014GL062018

Flato, G., Marotzke, J., Abiodun, B., Braconnot, P., Chou, S. C., Collins, W., et al. (2013). Evaluation of climate models. In T. F. Stocker, et al. (Eds.), *Climate change 2013: The physical science basis. Contribution of Working Group I to the Fifth Assessment Report of the Intergovernmental Panel on Climate Change*. Cambridge, UK: Cambridge University press.

Gourlan, A. T., Meynadier, L., Allègre, C. J., Tapponnier, P., Birck, J.-L., & Joron, J.-L. (2010). Northern Hemisphere climate control of the Bengali rivers discharge during the past 4 Ma. *Quaternary Science Reviews*, *29*(19–20), 2484–2498. https://doi.org/10.1016/j.quascirev.2010.05.003

Govin, A., Chiessi, C. M., Zabel, M., Sawakuchi, A. O., Heslop, D., Hörner, T., et al. (2014a). Terrigenous input off northern South America driven by changes in Amazonian climate and the North Brazil current retroflection during the last 250 ka. *Climate of the Past*, *10*(2), 843–862. https://doi.org/10.5194/cp-10-843-2014

Govin, A., Varma, V., & Prange, M. (2014b). Astronomically forced variations in western African rainfall (21°N–20°S) during the last interglacial period. *Geophysical Research Letters*, *41*, 2117–2125. https://doi.org/10.1002/2013GL058999

Guarino, M. V., Sime, L. C., Schroeder, D., Lister, G. M. S., & Hatcher, R. (2020). Machine dependence and reproducibility for coupled climate simulations: The HadGEM3-GC3.1 CMIP preindustrial simulation. *Geoscientific Model Development*, *13*, 139–154.

Hagemann, S. (2002). *An improved land surface parameter dataset for global and regional climate models*. Hamburg, Germany: Max-Planck-Institut für Meteorologie. Retrieved from https://www.mpimet.mpg.de/fileadmin/publikationen/Reports/max_scirep_336.pdf

Hagemann, S., Botzet, M., Dümenil, L., & Machenhauer, B. (1999). *Derivation of global GCM boundary conditions from 1 km land use satellite data*. Hamburg, Germany: Max-Planck-Institut für Meteorologie. Retrieved from https://www.mpimet.mpg.de/fileadmin/publikationen/Reports/max_scirep_289.pdf

Hersbach, H., Bell, W., Berrisford, P., Andras, H., Muñoz-Sabater, J., Nicolas, J., et al. (2019). Global reanalysis: Goodbye ERA-Interim, hello ERA5. *ECMWF Newsletter*, *159*.

Ikeuchi, H., Hirabayashi, Y., Yamazaki, D., Muis, S., Ward, P. J., Winsemius, H. C., et al. (2017). Compound simulation of fluvial floods and storm surges in a global coupled river-coast flood model: Model development and its application to 2007 Cyclone Sidr in Bangladesh. *Journal of Advances in Modeling Earth Systems*, *9*, 1847–1862. https://doi.org/10.1002/2017MS000943

Itambi, A. C., von Dobeneck, T., Mulitza, S., Bickert, T., & Heslop, D. (2009). Millennial-scale northwest African droughts related to Heinrich events and Dansgaard-Oeschger cycles: Evidence in marine sediments from offshore Senegal. *Paleoceanography*, *24*, PA1205. https://doi.org/10.1029/2007PA001570

Kiro, Y., Goldstein, S. L., Garcia-Veigas, J., Levy, E., Kushnir, Y., Stein, M., & Lazar, B. (2017). Relationships between lake-level changes and water and salt budgets in the Dead Sea during extreme aridities in the eastern Mediterranean. *Earth and Planetary Science Letters*, *464*, 211–226. https://doi.org/10.1016/j.epsl.2017.01.043

Knight, C. W., Dorale, J. A., & Edwards, R. L. (2006). *Stalagmite records of interglacial and glacial flooding at Crevice Cave*. Missouri, USA: American Geophysical Union, Fall Meeting 2006, abstract id. PP51D-1164.

Kujau, A., Nürnberg, D., Zielhofer, C., Bahr, A., & Röhl, U. (2010). Mississippi River discharge over the last ~560,000 years—Indications from X-ray fluorescence core-scanning. *Palaeogeography, Palaeoclimatology, Palaeoecology*, *298*(3–4), 311–318. https://doi.org/10.1016/j.palaeo.2010.10.005

Lehner, B., Verdin, K., & Jarvis, A. (2008). New global hydrography derived from spaceborne elevation data. *Eos, Transactions American Geophysical Union*, *89*(10), 93–94. https://doi.org/10.1029/2008EO100001

Loveland, T. R., Reed, B. C., Brown, J. F., Ohlen, D. O., Zhu, Z., Yang, L., & Merchant, J. W. (2000). Development of a global land cover characteristics database and IGBP DISCover from 1 km AVHRR data. *International Journal of Remote Sensing*, *21*(6–7), 1303–1330. https://doi.org/10.1080/014311600210191

Montero-Serrano, J.-C., Bout-Roumazeilles, V., Carlson, A. E., Tribovillard, N., Bory, A., Meunier, G., et al. (2011). Contrasting rainfall patterns over North America during the Holocene and last interglacial as recorded by sediments of the northern Gulf of Mexico. *Geophysical Research Letters*, *38*, L14709. https://doi.org/10.1029/2011GL048194

Nürnberg, D., Ziegler, M., Karas, C., Tiedemann, R., & Schmidt, M. W. (2008). Interacting loop current variability and Mississippi River discharge over the past 400 kyr. *Earth and Planetary Science Letters*, *272*(1–2), 278–289. https://doi.org/10.1016/j.epsl.2008.04.051

Olson, J. S. (1994a). *Global ecosystem framework-definitions* (p. *37*). Sioux Falls, SD. U.S.A.: USGS EROS Data Center Internal Report.

Olson, J. S. (1994b). *Global Ecosystem Framework-Translation Strategy* (p. 39). Sioux Falls, SD., U.S.A.: USGS EROS Data Center Internal Report.

Osborne, A. H., Marino, G., Vance, D., & Rohling, E. J. (2010). Eastern Mediterranean surface water Nd during Eemian sapropel S5: Monitoring northerly (mid-latitude) versus southerly (sub-tropical) freshwater contributions. *Quaternary Science Reviews*, *29*(19–20), 2473–2483. https://doi.org/10.1016/j.quascirev.2010.05.015

Otto-Bliesner, B. L., Braconnot, P., Harrison, S. P., Lunt, D. J., Abe-Ouchi, A., Albani, S., et al. (2017). The PMIP4 contribution to CMIP6—Part 2: Two interglacials, scientific objective and experimental design for Holocene and last interglacial simulations. *Geoscientific Model Development*, *10*, 3979–4003.

Pattan, J. N., Masuzawa, T., & Yamamoto, M. (2005). Variations in terrigenous sediment discharge in a sediment core from southeastern Arabian Sea during the last 140 ka. *Current Science*, *89*, 1421–1425.

Reheis, M. C., Bright, J., Lund, S. P., Miller, D. M., Skipp, G., & Fleck, R. J. (2012). A half-million-year record of paleoclimate from the Lake Manix Core, Mojave Desert, California. *Palaeogeography, Palaeoclimatology, Palaeoecology*, *365–366*, 11–37. https://doi.org/10.1016/j.palaeo.2012.09.002

Riboulleau, A., Bout-Roumazeilles, V., & Tribovillard, N. (2014). Controls on detrital sedimentation in the Cariaco Basin during the last climatic cycle: Insight from clay minerals. *Quaternary Science Reviews*, *94*, 62–73. https://doi.org/10.1016/j.quascirev.2014.04.023

Robert, C. (2004). Late Quaternary variability of precipitation in Southern California and climatic implications: Clay mineral evidence from the Santa Barbara Basin, ODP Site 893. *Quaternary Science Reviews*, *23*(9–10), 1029–1040. https://doi.org/10.1016/j.quascirev.2003.11.005

Sánchez Goñi, M. F., Eynaud, F., Turon, J. L., & Shackleton, N. J. (1999). High resolution palynological record off the Iberian margin: Direct land-sea correlation for the last interglacial complex. *Earth and Planetary Science Letters*, *171*(1), 123–137. https://doi.org/10.1016/S0012-821X(99)00141-7

Scussolini, P. (2014). Dynamics of Pleistocene climate change from the South Atlantic Ocean, PhD, Vrije Universiteit Amsterdam, Amsterdam. Retrieved from https://research.vu.nl/ws/portalfiles/portal/42135501/complete+dissertation.pdf

Simon, M. H., Ziegler, M., Bosmans, J., Barker, S., Reason, C. J. C., & Hall, I. R. (2015). Eastern South African hydroclimate over the past 270,000 years. *Scientific Reports*, *5*(1), 18,153. https://doi.org/10.1038/srep18153

Stuut, J.-B. W., Temmesfeld, F., & De Deckker, P. (2014). A 550 ka record of aeolian activity near North West Cape, Australia: Inferences from grain-size distributions and bulk chemistry of SE Indian Ocean deep-sea sediments. *Quaternary Science Reviews*, *83*, 83–94. https://doi.org/10.1016/j.quascirev.2013.11.003

van der Kaars, S., Miller, G. H., Turney, C. S. M., Cook, E. J., Nürnberg, D., Schönfeld, J., et al. (2017). Humans rather than climate the primary cause of Pleistocene megafaunal extinction in Australia. *Nature Communications*, *8*(1), 14142. https://doi.org/10.1038/ncomms14142

Weldeab, S., Lea, D. W., Schneider, R. R., & Andersen, N. (2007). 155,000 years of west African monsoon and ocean thermal evolution. *Science*, *316*(5829), 1303–1307. https://doi.org/10.1126/science.1140461

Winsemius, H. C., Aerts, J. C. J. H., van Beek, L. P. H., Bierkens, M. F. P., Bouwman, A., Jongman, B., et al. (2015). Global drivers of future river flood risk. *Nature Climate Change*, *6*, 381.

Wu, T., Lu, Y., Fang, Y., Xin, X., Li, L., Li, W., et al. (2019). The Beijing Climate Center Climate System Model (BCC-CSM): The main progress from CMIP5 to CMIP6. *Geoscientific Model Development*, *12*(4), 1573–1600. https://doi.org/10.5194/gmd-12-1573-2019

Xin, X., Wu, T., Zhang, J., Yao, J., & Fang, Y. (2020). Comparison of CMIP6 and CMIP5 simulations of precipitation in China and the East Asian summer monsoon. *International Journal of Climatology*.

Yamazaki, D., de Almeida, G. A. M., & Bates, P. D. (2013). Improving computational efficiency in global river models by implementing the local inertial flow equation and a vector-based river network map. *Water Resources Research*, *49*, 7221–7235. https://doi.org/10.1002/wrcr.20552

Yamazaki, D., O'Loughlin, F., Trigg, M. A., Miller, Z. F., Pavelsky, T. M., & Bates, P. D. (2014). Development of the Global Width Database for Large Rivers. *Water Resources Research*, *50*, 3467–3480. https://doi.org/10.1002/2013WR014664